

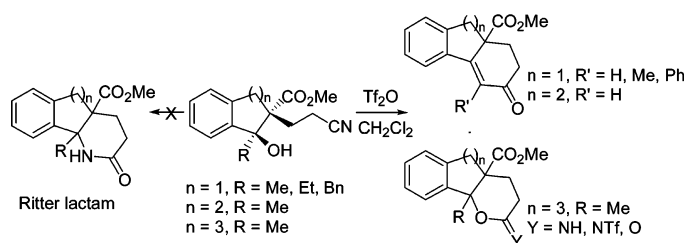
Studies on the Intramolecular Cyclizations of Bicyclic δ -Hydroxynitriles Promoted by Triflic Anhydride

Valeria Justribó, Silvina C. Pellegrinet,* and María I. Colombo*

Instituto de Química Orgánica y de Síntesis (CONICET), Facultad de Ciencias Bioquímicas y Farmacéuticas, Universidad Nacional de Rosario, Suipacha 531, Rosario (2000), Argentina

pellegrinet@iquios.gov.ar; colombo@iquios.gov.ar

Received December 28, 2006



Studies have been conducted to investigate the reactivity of several bicyclic δ -hydroxynitriles with triflic anhydride in dichloromethane. The reactions of the analogues derived from 1-indanone and 1-tetralone lead to annulated enones. These products arise from an initial elimination reaction that generates an alkene, followed by the addition of the carbon–carbon double bond to the activated cyano group. The intramolecular cyclization of the derivative obtained from 1-benzosuberone unexpectedly followed a different path, giving a cyclic imide as the major product. In this case, the activated cyano group is directly attacked by the hydroxyl group of the starting δ -hydroxynitrile. Theoretical calculations provide a rationale for the observed reactivity pattern. Both the formation of the triflate via its protonated form, its subsequent ionization to the carbocation, and the cyclization of the resulting alkene to the enone become less favorable when the size of the ring increases due to conformational effects. The opposite trend is observed for the competing Pinner-type cyclization to the imide. An alternative mechanism for the formation of the lactams from the cyclic imidates under acid-catalyzed conditions has also been proposed.

Introduction

The Ritter reaction consists of the nucleophilic attack of a nitrile to a carbocation, followed by hydrolysis to the corresponding amide.^{1,2} The carbocation is usually generated in strong acid media from an alcohol or an alkene.³ During the past years, Compennolle and co-workers have described a number of intramolecular Ritter reactions of hydroxynitriles under various acidic conditions as a means for preparing polycyclic lactam compounds.⁴ To shed light into some subtle mechanistic aspects of these reactions and to increase the yields of the products, we

have recently engaged in related studies.⁵ In particular, we aimed at using triflic anhydride to promote cyclizations under mild

* To whom correspondence should be addressed. Telephone/fax: +54-341-4370477.

(1) (a) Ritter, J. J.; Minieri, P. P. *J. Am. Chem. Soc.* **1948**, *70*, 4045. (b) Ritter, J. J.; Kalish, J. J. *J. Am. Chem. Soc.* **1948**, *70*, 4048.

(2) For reviews of the Ritter reactions, see: (a) Krimen, L. I.; Cota, D. J. In *Organic Reactions*; Dauben, W. G., Ed.; John Wiley & Sons: New York, 1969; Vol. 17, pp 213–325. (b) Bishop, R. In *Comprehensive Organic Synthesis*; Trost, B. M.; Fleming, I., Eds.; Pergamon Press: New York, 1991; Vol. 6, pp 261–300.

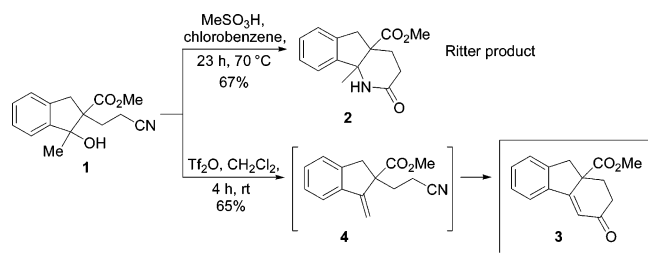
(3) For alternative methodologies developed for the Ritter reaction, see: (a) Top, S.; Jaouen, G. *J. Org. Chem.* **1981**, *46*, 78–82. (b) Barton, D. H. R.; Magnus, P. D.; Garbarino, J. A.; Young, R. N. *J. Chem. Soc., Perkin Trans. I* **1974**, 2101–2107. (c) Mukhopadhyay, M.; Iqbal, J. *J. Org. Chem.* **1997**, *62*, 1843–1845. (d) Chang, S. J. *Org. Process Res. Dev.* **1999**, *3*, 232. (e) Firouzabadi, H.; Sardarian, A. R.; Badparva, H. *Synth. Commun.* **2000**, *30*, 601–607. (f) Reddy, K. L. *Tetrahedron Lett.* **2003**, *44*, 1453–1455.

(4) (a) Van Emelen, K.; De Wit, T.; Hoornaert, G. J.; Compennolle, F. *Org. Lett.* **2000**, *2*, 3083–3086. (b) De Wit, T.; Van Emelen, K.; Maertens, F.; Hoornaert, G. J.; Compennolle, F. *Tetrahedron Lett.* **2001**, *42*, 4919–4922. (c) Van Emelen, K.; De Wit, T.; Hoornaert, G. J.; Compennolle, F. *Tetrahedron* **2002**, *58*, 4225–4236. (d) Maertens, F.; Van den Bogaert, A.; Compennolle, F.; Hoornaert, G. J. *Eur. J. Org. Chem.* **2004**, 4648–4656.

(5) Justribó, V., unpublished results.

(6) For the use triflic anhydride in intramolecular Ritter reactions, see: García Martínez, A.; Martínez Alvarez, R.; Teso Vilar, E.; García Fraile, A.; Hanack, M.; Subramanian, L. R. *Tetrahedron Lett.* **1989**, *30*, 581–582.

SCHEME 1

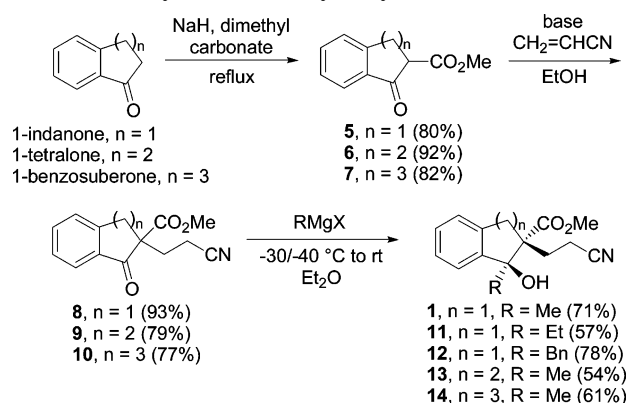


conditions.⁶ This reagent finds extensive application in organic synthesis due to its highly activating properties as well as its synthetic and mechanistic advantages.⁷ Preliminary results obtained in our laboratory clearly indicated that the choice of the reaction conditions in the cyclizations of some hydroxynitriles had a dramatic effect on the outcome of the reaction.⁸ In 2000, Compennolle reported that the reaction of bicyclic δ -hydroxynitrile **1** with methanesulfonic acid in chlorobenzene at 70 °C generated tricyclic lactam **2** in 67% yield (Scheme 1).^{4a} Later, we found that treatment of a dichloromethane solution of **1** with triflic anhydride at room temperature did not afford the classical product of the Ritter reaction. Instead, these conditions gave rise to tricyclic enone **3** in 65% yield via alkene **4**, which was formed in situ from alcohol **1** (Scheme 1).⁹

Examples of this class of chemical transformations in the literature are scarce. Hill, Conley, and co-workers described that the reactions of unsaturated nitriles with polyphosphoric acid at 120–130 °C led to α,β -unsaturated ketones known as Hoesch products.¹⁰ To the best of our knowledge, these are the only reports published to date that are related to the formation of enone **3**. In this context, we decided to further explore the triflic anhydride-promoted intramolecular cyclizations of δ -hydroxynitriles.

Results and Discussion

Triflic Anhydride-Promoted Intramolecular Cyclizations of δ -Hydroxynitriles. Our approach consisted of examining the reactions of different substrates that were likely to generate an alkene intermediate by a prompt elimination reaction of the starting alcohol. Consequently, all of the substrates included in this report are benzylic tertiary alcohols that have β hydrogen atoms.¹¹ The effect of the variation of the size of the aliphatic ring would also be investigated. Several bicyclic δ -hydroxynitriles were therefore synthesized, and their cyclization reactions were analyzed. The sequence previously developed by Comp-

SCHEME 2. Synthesis of δ -Hydroxynitriles **1** and **11–14**

ennolle for compound **1** was adapted to prepare the desired δ -hydroxynitriles (Scheme 2).^{4a} Carbomethoxylation of 1-indanone, 1-tetralone, and 1-benzosuberone using sodium hydride and dimethyl carbonate gave rise to β -ketoesters **5**, **6**, and **7**, respectively.¹² Subsequent treatment with a convenient base, such as triethylamine ($n = 1$) or aqueous sodium hydroxide solution ($n = 2$ and **3**), and acrylonitrile afforded the expected Michael adducts **8**, **9**, and **10** in high yields. This modification of the original technique, which employed sodium *tert*-butoxide as the base, reduced the reaction time from 72 to 3 h for compound **5**.¹³ In addition, the purification of sodium *tert*-butoxide by sublimation was avoided.

The synthesis of δ -hydroxynitriles **1** and **11–14** was performed by addition of the corresponding freshly prepared Grignard reagents in diethyl ether. These reactions occurred much faster in diethyl ether than in tetrahydrofuran (45 min vs overnight,^{4a} respectively, for the preparation of **1**). Moreover, use of diethyl ether guaranteed that the reactants remained in solution at low temperatures. Compennolle previously assigned the relative stereochemistry of hydroxynitrile **1** by comparison of NMR data and NOE experiments.^{4a} The methyl group and the cyanoethyl side chain were shown to have a *trans* relative orientation. This stereochemistry was proposed to arise from the formation of a Mg^{2+} chelate with the keto and the ester carbonyl groups, which is attacked by the nucleophile from the less hindered face, that is, opposite to the cyanoethyl group. Comparison of the ¹H NMR spectra and mechanistic reasoning suggest δ -hydroxynitriles **11–14** have the same relative stereochemistry. In addition, the spectra of these compounds showed a sharp singlet in the 2–3.5 ppm region that was assigned to the hydroxyl group. These signals did not shift with changes in concentration, which evidenced the alcohols exhibit an intramolecular hydrogen-bond interaction. Inspection of molecular models suggests the hydroxyl group can best hydrogen bond to the carbonyl oxygen of the ester moiety when these two groups are *trans*, which further supports the relative stereochemistry assigned to the δ -hydroxynitriles under study.

Substrates **11–14** were then subjected to the reaction with triflic anhydride in dichloromethane (Table 1). As for the

(7) For a review on triflic anhydride, see: Baraznenok, I. L.; Nenajdenko, V. G.; Balenkova, E. S. *Tetrahedron* **2000**, *56*, 3077–3119.

(8) Justribo, V.; Colombo, M. I. *Tetrahedron Lett.* **2003**, *44*, 8023–8024.

(9) Murakata, M.; Mizuno, Y.; Yamaguchi, H.; Hoshino, O. *Chem. Pharm. Bull.* **1999**, *47*, 1380–1383. In this publication, the (*S*)-enantiomer of enone **3** was described. This reference was unintentionally omitted in our previous publication (ref 8).

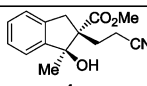
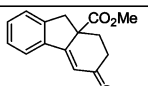
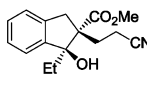
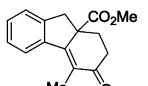
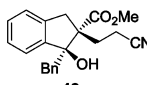
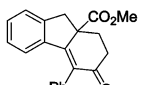
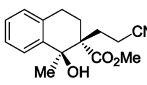
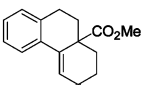
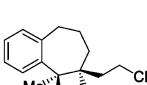
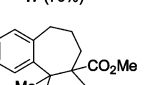
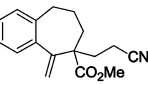
(10) (a) Hill, R. K.; Conley, R. T. *J. Am. Chem. Soc.* **1960**, *82*, 645–652. (b) Conley, R. T.; Lange, R. J. *J. Org. Chem.* **1963**, *28*, 210–214. (c) Hill, R. K.; Conley, R. T.; Chortyk, O. T. *J. Am. Chem. Soc.* **1965**, *87*, 5646–5651.

(11) To simplify the analysis presented in this paper, we have not included the results of the reactions of other δ -hydroxynitriles that have been synthesized in our laboratory (ref 5). These include a variety of acyclic and monocyclic substrates with secondary and tertiary alcohol functionalities. None of these δ -hydroxynitriles gave rise to enones upon treatment with triflic anhydride. The results of these experiments will be published elsewhere in due course.

(12) The reaction mixtures needed to be acidified with aqueous HCl solution during the workup because otherwise the isolation of products as described in ref 4a was difficult and the yields were low. For a reference, see: Anderson, A. G.; Greef, H. F. *J. Am. Chem. Soc.* **1952**, *74*, 5203–5204.

(13) This protocol was developed after much experimentation while working on the Michael addition of methyl 2-oxocyclopentanecarboxylate to acrylonitrile because use of typical bases led to the opening of the ring. For a reference, see: Adamcik, J. A.; Miklasiewicz, E. J. *J. Org. Chem.* **1963**, *28*, 336–339.

TABLE 1. Cyclization Reactions of δ -Hydroxynitriles **1** and **11**–**14**

Entry	δ -Hydroxynitrile	Reaction conditions	Products (Yields)
1 ^a		rt, 3 h, 1 equiv. Tf ₂ O	 3 (65%)
2		rt, 24 h, 1 equiv. Tf ₂ O	 15 (61%)
3 ^a		rt, 3 h, then reflux, 24 h, 2 equiv. Tf ₂ O	 16 (65%)
4		rt, 4.5 h, 1 equiv. Tf ₂ O	 17 (79%)
5		rt, 3 h, 1 equiv. Tf ₂ O	 18 , Y = NH (40 %) 19 , Y = O (11 %) 20 , Y = NTf (16 %)  21 (13%)

^a Traces of the intermediate alkenes were also isolated in these reactions.

reaction of δ -hydroxynitrile **1**, compounds **11**, **12**, and **13** gave the expected annulated enones **15**, **16**, and **17** (entries 1–4). However, and probably due to the steric hindrance imposed by the bulkier alkyl substituents, the reactions of substrates **11** and **12** required longer reaction times (entries 2 and 3). More vigorous conditions were also needed for **12** (higher temperature and 2 equiv of triflic anhydride). It is also interesting to point out that the cyclizations of δ -hydroxynitriles **11** and **12** initially gave complex reaction mixtures, but after column chromatography considerable quantities of enones **15** and **16** were obtained. Consequently, yields were optimized by stirring the crude reaction mixtures in dichloromethane with silica gel overnight before purification. The reaction of the six-membered ring analogue **13** occurred readily under standard conditions, giving rise to tricyclic enone **17** in 79% yield (entry 4). The cyclization of δ -hydroxynitrile **14** gave an interesting mixture of products (entry 5). After column chromatography on silica gel, a highly polar compound was isolated as the major product in 40% yield. The IR spectra of this product showed absorption bands at 1725 and 1660 cm⁻¹. In addition, two signals at 175.0 and 167.9 ppm were observed in the ¹³C NMR spectra. We first thought that a Ritter reaction had occurred and a lactam had been generated. However, the ¹³C NMR signal at 86.9 ppm clearly indicated that the benzylic quaternary carbon was attached to an oxygen atom rather than to a nitrogen. Based on this analysis, the major product was characterized as tricyclic imide **18**.

We later realized that compound **18** slowly decomposes upon standing, and also when treated with silica gel, giving rise to lactone **19**. Lactone **19** was obtained in 11% yield after column chromatography of the crude reaction mixture. The less polar products were isolated in 16% and 13% yield, and their structures were assigned to *N*-((trifluoromethyl)sulfonyl)imide **20** and alkene **21** based on spectroscopic methods and analytic data (see Supporting Information). Structure **20** belongs to a rare class of compounds because only a few examples of *N*-sulfonylimines and imide esters are known.¹⁴ The stretching band of the carbon–nitrogen double bond of **20** appeared at 1596 cm⁻¹ in the IR spectra. In addition, ¹³C NMR signals at 173.6, 118.9 (*J*_{C–F} = 319.3 Hz), and 93.9 ppm corresponding to C=N, CF₃, and C–O carbons further supported the structure proposed for **20**. To our surprise, *N*-((trifluoromethyl)sulfonyl)imide **20** exhibited high stability despite its electron-deficient nature. Traces of another highly polar compound that decomposed into lactone **19** were obtained, but, as a result of the low stability of this minor product, its structure could not be elucidated. We were not able to determine the relative stereochemistry of the ring-fused products originated in the cyclization of δ -hydroxynitrile **14** because NOE experiments did not provide useful information. However, on the basis of mechanistic grounds, we assume that relative stereochemistry is maintained during the course of the reaction so that *cis*-fused products are obtained.

The data gathered in Table 1 support the result previously obtained with δ -hydroxynitrile **1**.⁸ None of the triflic anhydride-promoted cyclizations of the substrates included in this study lead to Ritter lactams. Instead, under these conditions, different reaction pathways are followed. As shown for compounds **1**, **11**, **12**, and **13**, the formation of enones appears to be quite general for tertiary δ -hydroxynitriles derived from 1-indanone and 1-tetralone that have β hydrogens. In contrast, the seven-membered ring analogue **14** gave mainly a mixture of imides. The proposed mechanisms for the competitive cyclizations promoted by triflic anhydride are depicted in Scheme 3 for the methyl substituted δ -hydroxynitriles **1**, **13**, and **14**. Treatment of the starting alcohols with triflic anhydride might lead to intermediates **22**, **23**, and **24**, which, upon deprotonation, give rise to the corresponding triflates **25**, **26**, and **27**.¹⁵ Ionization of triflates **25**, **26**, and **27** should readily yield tertiary benzylic carbocations **28**, **29**, and **30**.¹⁶ If a proton is then lost from the methyl groups attached to the cationic carbons, alkenes **4**, **31**, and **21** are formed (path a). The resulting carbon–carbon double bond might subsequently act as a nucleophile attacking the cyano group (or, more likely, its activated form as in **32**, **33**, and **34**) to generate an imino group, leaving a tertiary carbocation adjacent to the aromatic ring (**35**, **36**, and **37**). Abstraction of an α proton and hydrolysis of the imine gives rise to α,β -unsaturated ketones **3**, **17**, and **38**.

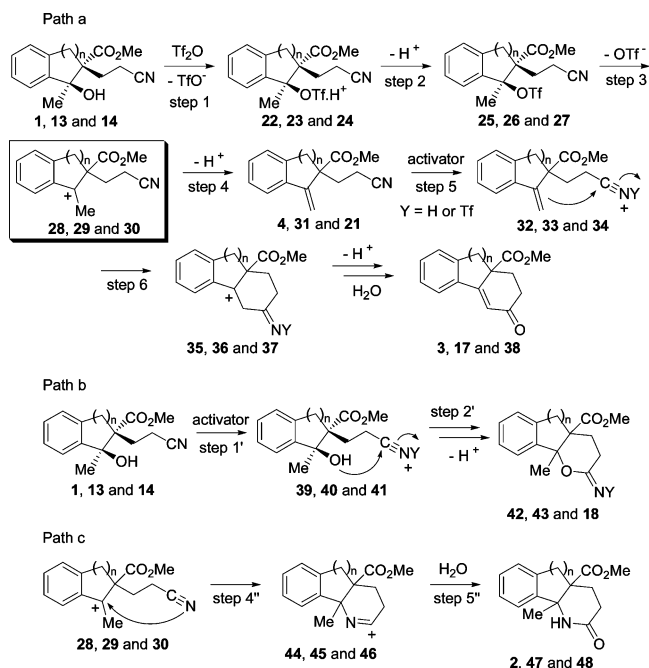
On the other hand, if the activated cyano group of intermediates **39**, **40**, and **41** is directly attacked by the hydroxyl group

(14) (a) Bundgaard, H.; Larsen, J. *J. Med. Chem.* **1988**, *31*, 2066–2069. (b) Böttger, G.; Geisler, A.; Fröhlich, R.; Würthwein, E.-U. *J. Org. Chem.* **1997**, *62*, 6407–6411.

(15) Overman, L. E.; Wolfe, J. P. *J. Org. Chem.* **2002**, *67*, 6421–6429 and references cited therein.

(16) Carbocations **28**–**30** could also be formed directly from intermediates **22**–**24**.

SCHEME 3. Proposed Mechanisms for the Competitive Cyclizations Promoted by Triflic Anhydride



of the starting δ -hydroxynitrile in a Pinner-type reaction,¹⁷ imidates **42**, **43**, and **18** are formed (path b). A third path has to be considered (path c). Nucleophilic attack of the cyano group onto the electrophilic carbon of the carbocations might generate cyclic nitrilium ions **44**, **45**, and **46**, which, upon hydrolysis, are converted into lactams **2**, **47**, and **48**. Path c corresponds to the classical Ritter reaction, which is not observed in any of the reactions described in this study.

To rationalize the observed reactivity pattern and to better understand the mechanism of the competitive cyclizations promoted by triflic anhydride, we have performed a theoretical study of the reactions of the methyl substituted δ -hydroxynitriles **1**, **13**, and **14**. Our main goal was to address the following issues: (1) Why do the reactions of δ -hydroxynitriles **1**, **11**, **12**, and **13** lead to enones? (2) Why does **14** cyclize to give imidates **18** and **20** as major products? (3) Why do none of these ring-closing reactions generate lactams?

Theoretical Calculations. We performed density functional theory (DFT) theoretical calculations using the B3LYP functional¹⁸ and the 6-31G* basis set¹⁹ unless otherwise noted. This method has been used to study many processes that involve carbocations.²⁰ Frequency calculations were used to confirm the nature of the stationary points. Natural bond orders (NBO)²¹ were calculated using the NBO program as implemented in Gaussian. Reported thermochemical properties include zero-point energies (ZPE) without scaling and were calculated at 1

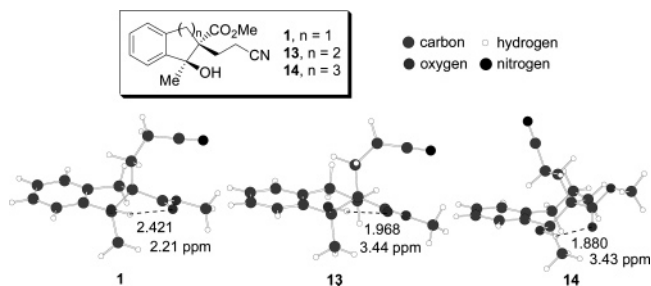


FIGURE 1. B3LYP/6-31G* geometries of δ -hydroxynitriles **1**, **13**, and **14**. Experimental ^1H NMR chemical shifts for the hydroxyl group and computed H–O distances (in Å) are also shown.

atm and 298.15 K. Free energies in solution were computed at the B3LYP/6-31G* level of theory on the structures optimized in the gas phase with the polarizable continuum model (PCM) as implemented in Gaussian 03 using dichloromethane as the solvent.²² All calculations were performed using Gaussian 98 and 03 packages.²³

The proposed competitive pathways shown in Scheme 3 were evaluated by locating key intermediates and calculating reaction energies and selected energy barriers. The conformers of minimum energy of the studied intermediates were located by performing systematic conformational searches at the RHF/3-21G level of theory and then reoptimizing selected minima with B3LYP/6-31G*. In many cases, a large number of initial geometries were generated using the conformational search module of Hyperchem²⁴ with the MM+ method.²⁵

Figure 1 depicts the geometries of the global minima found for the starting δ -hydroxynitriles **1**, **13**, and **14**. The most striking feature of these structures is that the computed distances between the hydrogen of the hydroxyl group and the carbonyl oxygen of the ester moiety are significantly shorter than the sum of their van der Waals radii. This observation suggests **1**, **13**, and **14** present intramolecular six-membered ring hydrogen-bonding interactions, which is supported by the ^1H NMR data mentioned above. Apparently, these interactions lock the conformation of the aliphatic ring because ring-flipping leads to higher energy conformations with a pseudo trans diaxial relationship for the hydroxyl and the ester groups, which cannot hydrogen bond. We have found other conformers of low energy, particularly for **1**, which differ mainly in the conformation of the side chain. However, the global minima seem to favor the hydrogen-bonding interactions and also to minimize the steric clashes

(17) Roger, R.; Neilson, D. G. *Chem. Rev.* **1961**, *61*, 179–211 and references cited therein.

(18) (a) Becke, A. D. *J. Chem. Phys.* **1993**, *98*, 5648–5652. (b) Lee, C.; Yang, W.; Parr, R. *Phys. Rev. B* **1988**, *37*, 785–789.

(19) Hehre, W. J.; Radom, L.; Schleyer, P. v. R.; Pople, J. A. *Ab Initio Molecular Orbital Theory*; Wiley: New York, 1986.

(20) (a) Martinez, A. G.; Vilar, E. T.; Barcina, J. O.; de la Moya Cerero, S. *J. Org. Chem.* **2005**, *70*, 10238–10246. (b) Gutta, P.; Tantillo, D. J. *J. Am. Chem. Soc.* **2006**, *128*, 6172–6179 and references cited therein.

(21) (a) Reed, A. E.; Weinstock, R. B.; Weinhold, F. *J. Chem. Phys.* **1985**, *83*, 735–746. (b) Reed, A. E.; Curtiss, L. A.; Weinhold, F. *Chem. Rev.* **1988**, *88*, 899–926.

(22) (a) Miertus, S.; Scrocco, E.; Tomasi, J. *Chem. Phys.* **1981**, *55*, 117–129. (b) Mennucci, B.; Tomasi, J. *J. Chem. Phys.* **1997**, *106*, 5151–5158.

(23) Frisch, M. J.; Trucks, G. W.; Schlegel, H. B.; Scuseria, G. E.; Robb, M. A.; Cheeseman, J. R.; Montgomery, J. A., Jr.; Vreven, T.; Kudin, K. N.; Burant, J. C.; Millam, J. M.; Iyengar, S. S.; Tomasi, J.; Barone, V.; Mennucci, B.; Cossi, M.; Scalmani, G.; Rega, N.; Petersson, G. A.; Nakatsuji, H.; Hada, M.; Ehara, M.; Toyota, K.; Fukuda, R.; Hasegawa, J.; Ishida, M.; Nakajima, T.; Honda, Y.; Kitao, O.; Nakai, H.; Klene, M.; Li, X.; Knox, J. E.; Hratchian, H. P.; Cross, J. B.; Adamo, C.; Jaramillo, J.; Gomperts, R.; Stratmann, R. E.; Yazyev, O.; Austin, A. J.; Cammi, R.; Pomelli, C.; Ochterski, J. W.; Ayala, P. Y.; Morokuma, K.; Voth, G. A.; Salvador, P.; Dannenberg, J. J.; Zakrzewski, V. G.; Dapprich, S.; Daniels, A. D.; Strain, M. C.; Farkas, O.; Malick, D. K.; Rabuck, A. D.; Raghavachari, K.; Foresman, J. B.; Ortiz, J. V.; Cui, Q.; Baboul, A. G.; Clifford, S.; Cioslowski, J.; Stefanov, B. B.; Liu, G.; Liashenko, A.; Piskorz, P.; Komaromi, I.; Martin, R. L.; Fox, D. J.; Keith, T.; Al-Laham, M. A.; Peng, C. Y.; Nanayakkara, A.; Challacombe, M.; Gill, P. M. W.; Johnson, B.; Chen, W.; Wong, M. W.; Gonzalez, C.; Pople, J. A. *Gaussian 03*, revision 6.1; Gaussian, Inc.: Pittsburgh, PA, 2003.

(24) *Hyperchem Professional Release 7.52*; Hypercube, Inc., 2005.

(25) Allinger, N. L. *J. Am. Chem. Soc.* **1977**, *99*, 8127–8134.

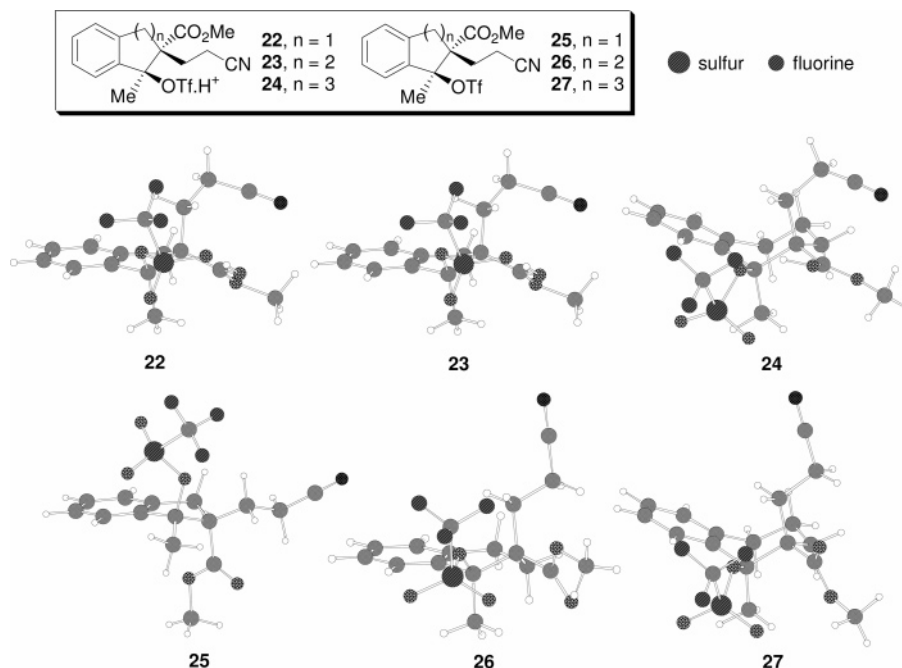


FIGURE 2. B3LYP/6-31G* geometries of protonated triflates **22**, **23**, and **24** and triflates **25**, **26**, and **27**. See Figure 1 for key.

between substituents. It is interesting to point out that the hydrogen—oxygen distances decrease considerably with increasing ring size. Inspection of the calculated geometries suggests that this effect could be attributed to the greater facility of the six- and seven-membered ring analogues for adopting conformations with the optimal bond angles for the hydrogen-bonding interactions to occur.

We then optimized the geometries of intermediates **22**, **23**, and **24** and the derived triflates **25**, **26**, and **27** (Figure 2).²⁶ The geometries of protonated triflates **22**, **23**, and **24** resemble those of the starting δ -hydroxynitriles **1**, **13**, and **14**, particularly for the five- and six-membered ring analogues where the side chain adopts the same conformation. However, the proton of the hydrogen-bonded hydroxyl group is now closer to the carbonyl oxygen of the ester functionality. Note that the conformation of the aliphatic ring of triflates **25**, **26**, and **27** changes only for the five-membered ring analogue, which now puckers toward the bottom face. The six- and seven-membered ring analogues maintain the conformation of the aliphatic ring, possibly to accommodate the triflate and carboxylate groups in pseudo equatorial positions. Also, the side chains of compounds **25**, **26**, and **27** adopt conformations, which minimize the steric repulsion between the triflate group and the pseudoaxial hydrogen of the ring.

The computed reaction free energies for the formation of protonated intermediates **22**, **23**, and **24** and triflates **25**, **26**, and **27** (ΔG_1 and ΔG_2 , respectively) from the corresponding alcohols (steps 1 and 2, Scheme 3) are shown in Figure 3. This figure depicts the energy profile for the generation of alkenes **4**, **31**, and **21** from δ -hydroxynitriles **1**, **13**, and **14** in the gas phase and in solution (steps 1–4, Scheme 3). It is interesting to remark that the calculated energy changes in solution are much lower than those in the gas phase because in the first case stabilization of the charged intermediates by solvation is

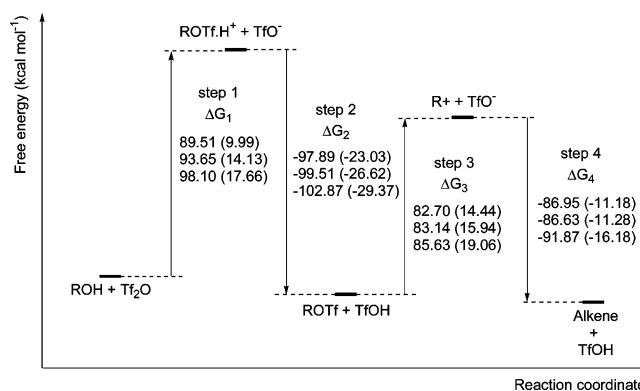


FIGURE 3. B3LYP/6-31G* energy profiles for the generation of alkenes **4**, **31**, and **21** from δ -hydroxynitriles **1**, **13**, and **14** (steps 1–4, path a, Scheme 3). Energy values are given in kcal mol⁻¹ from top to bottom for the five-, six-, and seven-membered ring analogues, respectively. Free energies in solution are also shown (in parentheses).

taken into account. However, the reaction energies obtained with both methods follow the same trends, and relative energies are similar for all steps. The computed reaction energies for step 1 (ΔG_1) suggest that, when the size of the aliphatic ring increases, the formation of the protonated triflate is less favorable. We believe both the increased stability of the starting δ -hydroxynitrile **14** due to the presence of a strong hydrogen bond and the lower stability of the highly congested resulting intermediate contribute to make the formation of **24** less favorable. Deprotonation of protonated triflates **22**, **23**, and **24** is predicted to be highly favorable in all cases, and computed values of ΔG_2 decrease with increasing ring size.

We then turned our attention to the carbocation intermediates generated in the ionization of triflates **25**, **26**, and **27** (step 3, Scheme 3). The geometries of the conformers of minimum energy for carbocations **28**, **29**, and **30** are very interesting (Figure 4). In this case, the nitrile side chain and the ester group are oriented in a similar fashion in all of the structures. On the other hand, while the five-membered ring of **28** is almost planar,

(26) Location of protonated triflates **22**, **23**, and **24** was somewhat complicated because many conformers dissociated to the corresponding carbocations plus triflic acid during minimizations.

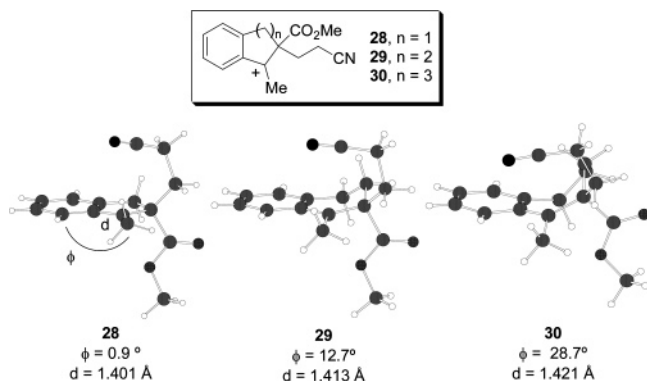


FIGURE 4. B3LYP/6-31G* geometries of carbocations **28**, **29**, and **30**. Torsion angles (ϕ) and carbon–carbon distances (d) are also shown. See Figure 1 for key.

the six- and seven-membered rings of **29** and **30** exhibit increasing puckering toward the top face. These peculiar conformations seem to be stabilized by an electronic interaction experienced between the electron-deficient carbon and the cyano group. This effect was confirmed by performing NBO calculations, which also evidenced that the donation of electron density from the cyano group to the carbocation carbon decreased with increasing ring size. Moreover, FMO calculations suggest the MOs related to the cyano groups of carbocations **28**, **29**, and **30** have lower energies than the calculated energy for the HOMO of acetonitrile (ca. -0.447 vs -0.326 eV), which supports the contribution of the proposed electronic interaction to the stabilization of these species.

In addition, the calculated C–C–C–C torsion angles between the methyl group and the aromatic carbon (ϕ) increase considerably as the size of the ring increases, indicating that the seven-membered ring carbocation **30** should be less stabilized by conjugation with the aromatic ring. The computed carbon–carbon distances (d) are in accordance with this observation because the higher is the distance, the lower is the conjugation. The increasing deviation from the plane might be attributed to a repulsive van der Waals interaction experienced between the methyl group and the proximate aromatic hydrogen. When the size of the ring increases, these groups become closer, so the torsion angle is increased to reduce this destabilizing interaction. These results are further supported by the higher energy calculated for the LUMO of carbocation **30**, together with its increased atomic coefficient on the positive carbon.

The computed reaction energies for the ionization of triflates **25**, **26**, and **27** to carbocations **28**, **29**, and **30** plus triflate ion (step 3, Scheme 3) increase with increasing ring size (ΔG_3 , Figure 3). This is in good agreement with the geometry features of the studied carbocations. When the conjugation with the aromatic ring decreases, the formation of the carbocation becomes less favorable.

The geometries of alkenes **4**, **31**, and **21** were then inspected. Several low-energy structures exhibiting different conformations for the aliphatic ring and the side chain were located for each compound. Contrary to the result obtained with the starting alcohols, conformers arising from ring-flipping of the aliphatic ring seem to be possible for the alkenes. Figure 5 shows the geometries of the global minima of alkenes **4**, **31**, and **21**. Apparently, when the methyl is transformed into a methylene, the deviation from the plane becomes more important. If the carbon–carbon double bond and the aromatic ring lie in the

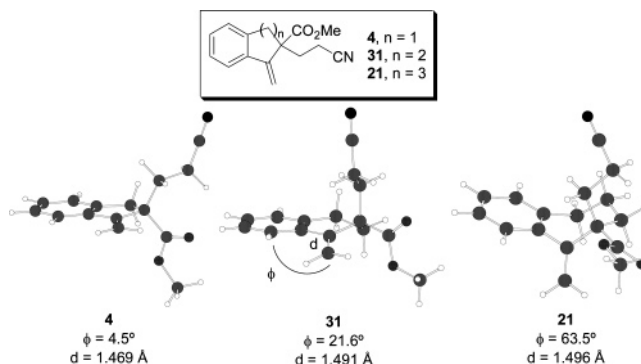


FIGURE 5. B3LYP/6-31G* geometries of alkenes **4**, **31**, and **21**. Torsion angles (ϕ) and carbon–carbon distances (d) are also shown. See Figure 1 for key.

same plane, one of the vinylic protons becomes closer to the proximal aromatic proton, so the alkenes adopt nonplanar conformations to avoid this repulsive steric effect. As a consequence, conjugation is lost to a greater extent in the deprotonation of carbocations, as revealed by the calculated torsion angles between the methylene carbon and the aromatic carbon (ϕ) and the carbon–carbon distances (d) of alkenes **4**, **31**, and **21**. This effect is significantly more important for the seven-membered ring analogue **21**, which has a torsion angle of 63.5° . The HOMOs of alkenes **4**, **31**, and **21** are -0.229 , -0.233 , and -0.240 eV, respectively, and the coefficients of this MO on the terminal sp^2 carbon decrease with increasing ring size. Although the differences between these values are small, they suggest that the nucleophilic character of the carbon–carbon double bond decreases from compound **4** to **31** to **21**, which might be related to the relative rates for the cyclization leading to the enones (step 6, Scheme 3).

We have also computed the reaction free energies for the deprotonation reactions of carbocations **28**, **29**, and **30** with triflate ion as the base to alkenes **4**, **31**, and **21**, respectively (step 4, Scheme 3). Deprotonation of the seven-membered ring analogue **30** seems to be more favorable than those of **28** and **29** (Figure 3). This could be attributed to the lower stability of the starting carbocation because the lack of conjugation should destabilize the carbocations more than their corresponding alkenes due to the higher electron deficiency of a positively charged carbon than that of an sp^2 carbon.

Calculated free energies shown in Figure 3 suggest the reaction rates of steps 1 and 3 (path a, Scheme 3) should decrease progressively along the series of compounds derived from 1-indanone, 1-tetralone, and 1-benzosuberone. Both the formation of the protonated triflate and the ionization of the triflate to the carbocation become less favorable when the size of the ring increases. This might influence the behavior of the seven-membered δ -hydroxynitrile **14** because formation of imide **18** (path b, Scheme 3) is favored over elimination to alkene **21**. Similar structural effects have been observed in several reactions of other indanone, tetralone, and benzosuberone derivatives.²⁷ Conformational effects arising from the introduction of sp^2 carbons in the aliphatic rings appear to have a great influence on the reactivity by affecting the conjugation of key

(27) (a) Streitwieser, A. *Chem. Rev.* **1956**, *56*, 571–752. (b) Eldin, S.; Pollack, R. M.; Whalen, D. L. *J. Am. Chem. Soc.* **1991**, *113*, 1344–1349. (c) Eldin, S.; Dale, L.; Pollack, R. M. *J. Org. Chem.* **1993**, *58*, 3490–3495. (d) Bowman, W. R.; Westlake, P. J. *Tetrahedron* **1992**, *49*, 4027–4038.

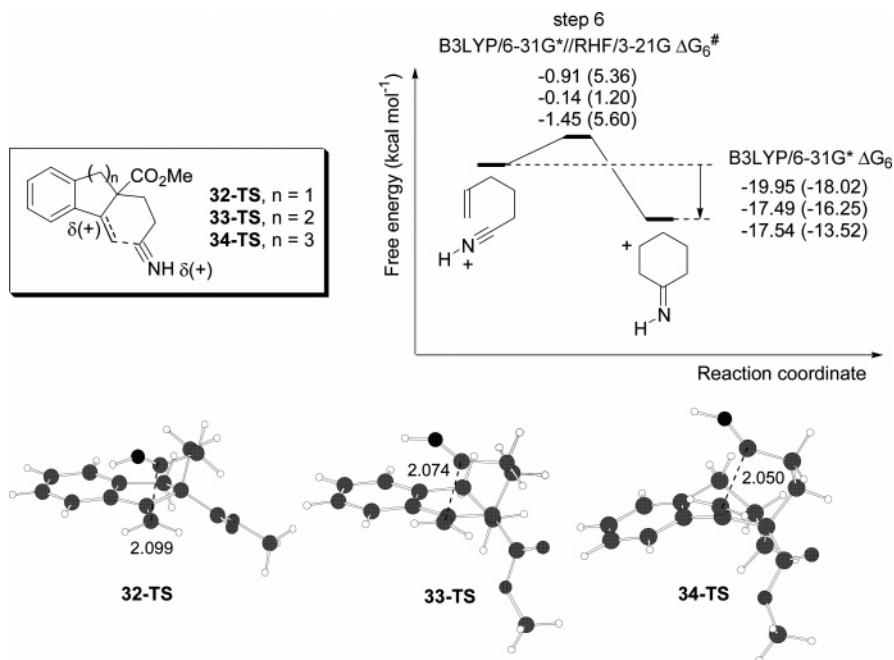


FIGURE 6. Energy profiles for the cyclization step leading to enones (step 6, Scheme 3). Energies are given in kcal mol⁻¹ from top to bottom for the five-, six-, and seven-membered ring analogues, respectively. Free energies in solution are given in parentheses. RHF/3-21G geometries of **32-TS**, **33-TS**, and **34-TS** with carbon–carbon distances (in Å) are also shown. See Figure 1 for key.

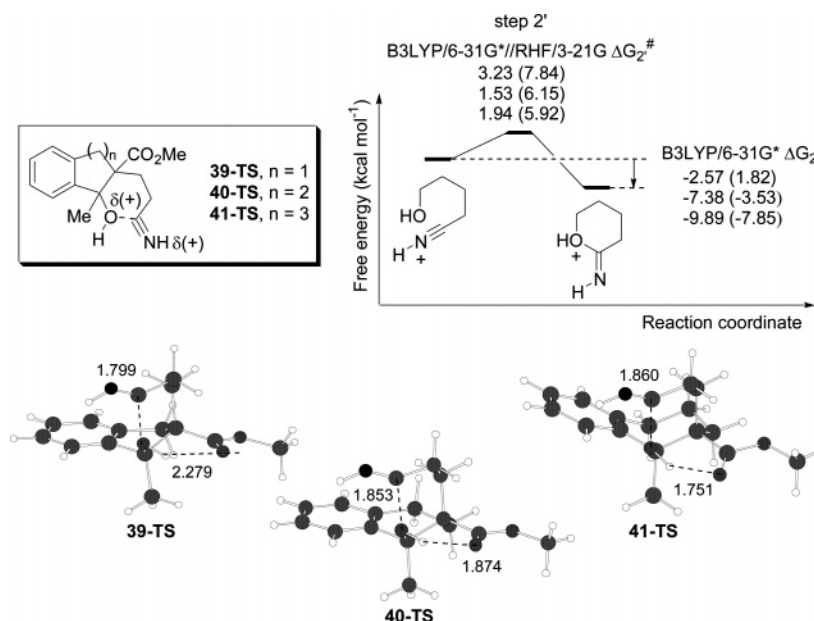


FIGURE 7. Energy profiles for the cyclization step leading to imidates (step 2', Scheme 3). Energies values are given in kcal mol⁻¹ from top to bottom for the five-, six-, and seven-membered ring analogues, respectively. Free energies in solution are given in parentheses. RHF/3-21G geometries of **39-TS**, **40-TS**, and **41-TS** with carbon–oxygen and hydrogen–oxygen distances (in Å) are also shown. See Figure 1 for key.

intermediates. In our case, the slower rate of the dehydration of δ -hydroxynitrile **14** is probably related to the conformational requirements imposed by the seven-membered ring, which prevent the developing carbocation from achieving coplanarity with the aromatic ring.

We next studied the cyclization steps of pathways a–c (steps 6, 2', and 4'', Scheme 3). We have located the transition structures for the cyclization leading to the enones (step 6, path a) and to the imidates (step 2', path b) at the RHF/3-21G level

of theory using a proton as the activator (Figures 6 and 7).²⁸ On the other hand, all of the attempts to locate the Ritter transition structures for the attack of the cyano group to the carbocation carbon (step 4'', path c) failed, systematically moving the side chain away from the electron-deficient center and leading to the starting carbocations. Inspection of molecular models clearly

(28) All located transition structures had only one imaginary frequency corresponding to the formation of the expected bonds.

shows that the intramolecular attack of the nitrogen of the linear cyano group to the carbocation leads to the cyclic nitrilium ions through highly strained transition structures.^{2b,10a} An intriguing point is that the cyclization of δ -hydroxynitrile **1** in protic acids does give rise to lactam **2** (Scheme 1).^{4a} This result suggests that a different mechanism might operate in this type of intramolecular transformation (vide infra).

The potential energy surfaces for the studied cyclization reactions seem to be very flat because the attempts we made to locate the B3LYP/6-31G* transition structures failed leading either to the reactants or to the cyclic products. The computed B3LYP/6-31G* single point energies of the transition structures located with the RHF/3-21G method provide an approximation to analyze reactivity trends. To calculate the activation energies and the reaction energies, we have also optimized the structures for the reactants and the ring-closed intermediates at the B3LYP/6-31G* level of theory (see Supporting information).

The transition structures for the cyclization reaction leading to the enones (step 6, path a) exhibit highly ordered chairlike geometries (Figure 6). The corresponding boatlike transition structures were calculated to have much higher energy. We have also studied the isomerization of the developing imino group by changing the position of the hydrogen atom, and the Z configuration was predicted to be more stable. Carbon–carbon distances appear to decrease smoothly with increasing ring size from 2.099 for **32-TS** to 2.050 Å for **34-TS**. Calculated B3LYP/6-31G*/RHF/3-21G free energy barriers in the gas phase and in solution are extremely low,²⁹ suggesting the cyclizations of the alkenes should occur easily.³⁰ In addition, B3LYP/6-31G* reaction free energies for the cyclization reaction leading to the enones become less favorable with increasing ring size. These results can be rationalized by considering the geometries of ring-closed products. The cyclic products have a positively charged carbon adjacent to the aromatic ring so their energy should be influenced by the degree of conjugation with the aromatic ring, which should ultimately affect the equilibrium constant for this cyclization step. These calculations show that both the dehydration of the δ -hydroxynitrile and the intramolecular cyclization of the resulting alkene are less favorable for the seven-membered ring analogue **14**.

The transition structures for the cyclization leading to the imidates via a Pinner-type reaction (step 2', path b) exhibit highly ordered chairlike geometries as well (Figure 7). It is interesting to point out that these transition structures present stabilizing hydrogen-bonding interactions. The strength of such interactions increases along the series **39-TS**, **40-TS**, and **41-TS** and might be related to the observed increased reactivity of the seven-membered δ -hydroxynitrile **14** toward path b. Fur-

thermore, the calculated carbon–oxygen distances increase smoothly with increasing ring size from 1.799 for **39-TS** to 1.860 Å for **41-TS**.

The activation free energies for this step both in the gas phase and in solution are computed to be very small. General trends indicate that the activation and reaction free energies for the attack of the hydroxyl group to the activated cyano group decrease when the size of the ring increases. This might be related to the experimental fact that the seven-membered analogue **14** is the only compound that suffers a cyclization reaction involving the hydroxyl group.

The theoretical results presented thus far give relative trends that seem to be important in the competition between pathways a and b in Scheme 3. However, they do not fully explain why the reactions of the five- and six-membered δ -hydroxynitriles lead to enones via the corresponding alkenes while the seven-membered analogue mainly follows a Pinner-type pathway to the imideate.

The key to understanding the competition between the enone and the imideate routes seems to be related to the initial activation step of the starting δ -hydroxynitriles.³¹ Calculations suggest that all of the different activation steps, that is, formation of the protonated triflates or protonation of either the hydroxyl or the cyano groups, are energetically plausible (Figures 3 and 8).³² However, for the five- and six-membered analogues, attack of the hydroxy group onto triflic anhydride to form the corresponding protonated triflates seems to be more favorable than protonation. The protonated triflates are then deprotonated to give the corresponding triflates, which ionize to the carbocations and triflate ion. Deprotonation of the carbocations then generates the respective alkenes, which readily cyclize to the enones (Figure 6).

Computed energy trends suggest that the formation of the protonated triflate becomes less favorable with increasing ring size (step 1, Figure 3), while protonation of the alcohol is more favorable (Figure 8). The properties of the starting δ -hydroxynitriles appear to be responsible for this behavior. Although the seven-membered alcohol **14** presents the stronger hydrogen-bond interaction and exhibits the greater nucleophilicity, it is highly hindered. Consequently, it seems to prefer to be protonated rather than triflated. Afterward, the protonated alcohol could lose a molecule of water to give the carbocation or act as a Brønsted acid to protonate the cyano group. Energetics suggest the latter process is more favorable. The protonated nitrile thus generated then cyclizes easily via a Pinner-type mechanism to give the protonated imideate in a thermodynamically favorable reaction (Figure 7).

Figure 9 shows the geometries of the protonated alcohols **49**, **50**, and **51**, which are very much like the protonated triflates **22**, **23**, and **24**. Note that the aliphatic rings and side chains adopt the same conformation and also that the proton of the

(29) The negative sign of the computed activation energies might be a consequence of the flatness of the PES and also of the method employed in the calculations because B3LYP is known to underestimate energy barriers. For some recent references, see: (a) Pemberton, R. P.; McShane, C. M.; Castro, C.; Karney, W. L. *J. Am. Chem. Soc.* **2006**, *128*, 16692–16700. (b) Jee, J.; Tao, F.-M. *J. Phys. Chem. A* **2006**, *110*, 7682–7689. (c) Voegelé, A. F.; Tautermann, C. S.; Loerting, T.; Liedl, K. R. *J. Phys. Chem. A* **2002**, *106*, 7850–7857. (d) Dibble, T. S. *J. Phys. Chem. A* **2002**, *106*, 6643–6650. (e) Gonzales, J. M.; Cox, R. S., III; Brown, S. T.; Allen, W. D.; Schaefer, H. F., III. *J. Phys. Chem. A* **2001**, *105*, 11327–11346 and references cited therein.

(30) Because the studied protonations appear to be considerably demanding in terms of energy, they should be taken into account to evaluate the feasibility of the cyclizations to the enones. Calculated free reaction energies in dichloromethane for the protonation of the carbon–carbon double bonds of the alkenes with triflic acid are ca. 20 kcal mol⁻¹, suggesting that these processes should be energetically feasible at room temperature.

(31) Activation of the cyano group by protonation has been shown to be the rate-limiting step in some reactions involving nucleophilic attack on nitriles. For example, see: Himo, F.; Demko, Z. P.; Noodleman, L.; Sharpless, K. B. *J. Am. Chem. Soc.* **2002**, *124*, 12210–12216 and references cited therein.

(32) The localization of the transition structures leading to the protonation of the alcohols and the formation of the protonated triflates would lead to a clearer picture of the competence observed between these processes. However, based on Hammond's Postulate, transition structures should be closer in energy to the products than to the reactants because we computed both activation steps to be endergonic ($\Delta G > 0$). Reaction energies were thus used to estimate the reactivity trend for each process.

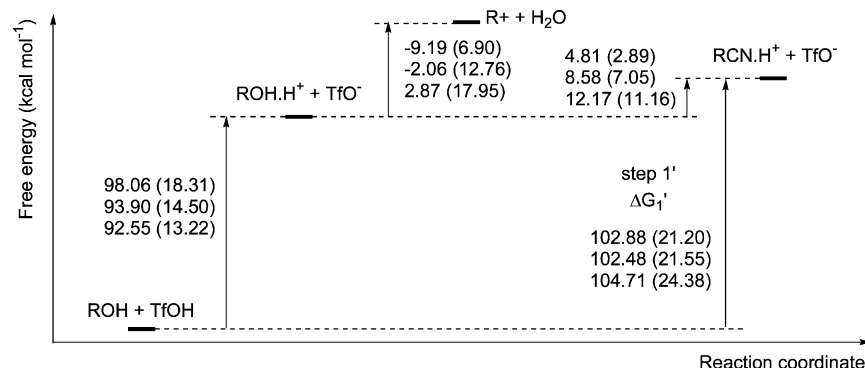


FIGURE 8. B3LYP/6-31G* energy profiles for the generation of the protonated hydroxynitriles **39**, **40**, and **41** from δ -hydroxynitriles **1**, **13**, and **14** (path b, Scheme 3). Energy values are given in kcal mol⁻¹ from top to bottom for the five-, six-, and seven-membered ring analogues, respectively. Free energies in solution are also shown (in parentheses).

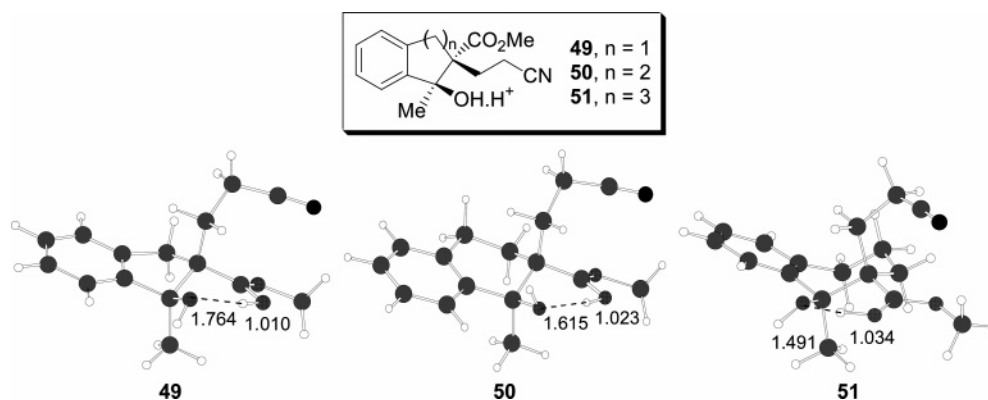
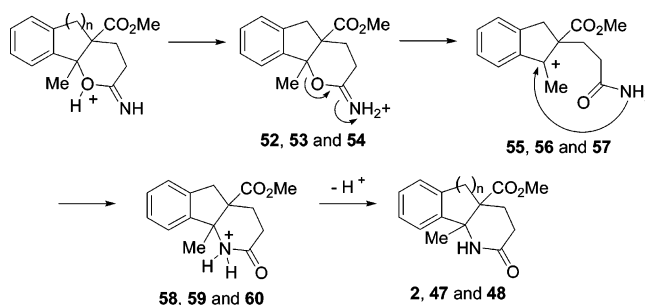


FIGURE 9. B3LYP/6-31G* geometries of protonated alcohols **49**, **50**, and **51**. Computed oxygen-hydrogen distances (in Å) are also shown. See Figure 1 for key.

hydrogen-bonded hydroxyl group is now closer to the carbonyl oxygen of the ester.³³

Finally, we investigated a possible alternative mechanism to account for the formation of the Ritter lactam **2** under Compemolle's conditions.^{4a} Because the Pinner cyclization was calculated to be readily accessible in terms of energy, one possibility is that under acid-catalyzed conditions imidates are initially formed, and, subsequently, they rearrange to the corresponding lactams as shown in Scheme 4.^{17,34,35} The imidates and the lactams should be the kinetic and thermodynamic products, respectively.³⁶ In our case, the Pinner imidates might isomerize to the lactams via an initial proton transfer to isomeric intermediates **52**, **53**, and **54**, followed by the ring opening to the benzylic carbocations **55**, **56**, and **57**. These carbocations have an ambident amide functional group, which could cyclize back to the protonated imidate or to the protonated lactams **58**, **59**, and **60** by intramolecular nucleophilic attack of

SCHEME 4. Proposed Alternative Mechanism for the Formation of Lactams



the oxygen or the nitrogen, respectively.^{35,37} Deprotonation of protonated lactams **58**, **59**, and **60** yields lactams **2**, **47**, and **48**.

Figure 10 shows the energy profiles for the conversion of the protonated imidates to protonated lactams **58**, **59**, and **60** and the geometries of the transition structures. Surprisingly, when we carried out the conformational searches for the studied intermediates, we observed that geometry optimizations of the lower energy conformers of carbocations **55**, **56**, and **57** spontaneously cyclized to protonated imidates **52**, **53**, and **54**. In addition, IRC (intrinsic reaction coordinate) analysis demonstrated that, instead of arising from the carbocations, the transition structures that lead to the protonated lactams **58**, **59**, and **60** (**55-TS**, **56-TS**, and **57-TS**) were connected directly to

(33) Cleavage of protonated alcohols to the carbocations and water was observed during some geometry optimizations. The same results have been obtained in a number of studies. For example, see: Fujio, M.; Keeffe, J. R.; More O'Ferrall, R. A.; O'Donoghue, A. C. *J. Am. Chem. Soc.* **2004**, *126*, 9982–9992.

(34) It is well known that imidates rearrange readily to amides. This rearrangement has been extensively studied and is known as the Chapman or Lander rearrangement depending on the nature of the carbon that shifts from the oxygen to the nitrogen. The mechanism of this reaction also appears to depend on the nature of the substituent.

(35) L'abbe, G. *Chem. Rev.* **1969**, *69*, 345–363.

(36) Martín, A.; Perez-Martín, I.; Suárez, E. *Org. Lett.* **2005**, *7*, 2027–2030.

(37) For a related attack of an ambident nucleophile see: Peng, Z.-H.; Woerpel, K. A. *Org. Lett.* **2001**, *3*, 675–678.

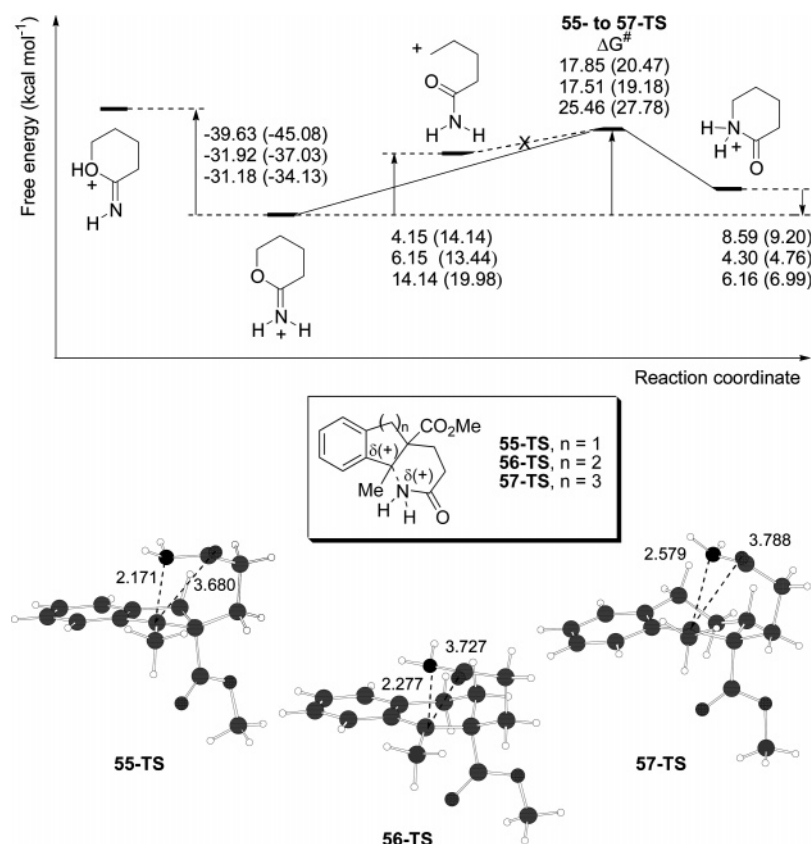


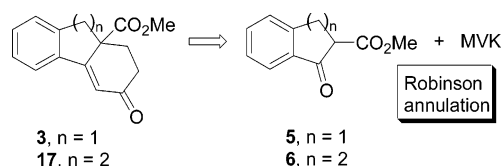
FIGURE 10. B3LYP/6-31G* energy profiles for the generation of protonated lactams **58**, **59**, and **60** from the protonated imidates (Scheme 4). Energy values are given in kcal mol⁻¹ from top to bottom for the five-, six-, and seven-membered ring analogues, respectively. Free energies in solution are given in parentheses. B3LYP/6-31G* geometries of **55-TS**, **56-TS**, and **57-TS** with carbon–nitrogen and carbon–oxygen distances (in Å) are also shown. See Figure 1 for key.

the protonated imidates **52**, **53**, and **54**. Therefore, the imidates under study seem to be likely to rearrange to the lactams through an alkyl 1,3-shift.³⁸

The located transition structures show that the proposed 1,3-shift should be much easier than the classical Ritter attack of the nitrile in carbocations **28**, **29**, and **30** due to the change in hybridization of the carbon and the nitrogen atoms (path c, Scheme 3). Transition structures **55- to 57-TS** are free from strain and also have an optimal orientation of the lone pair of the nitrogen to interact with the electrophilic carbon. The higher steric hindrance of **57-TS** might account for the higher activation energy calculated for the isomerization of the seven-membered ring analogue. It is interesting to remark though that the proposed mechanism for the formation of the lactams from the imidates exhibits feasible reactions free energies and activation barriers. Consequently, under thermodynamic conditions, such as those used by Compennolle, this transformation should take place without difficulty.

The results of the study described in this paper suggest the scope of the reported methodology for the synthesis of annulated enones might be limited to δ -hydroxynitriles that dehydrate readily. Furthermore, the resulting alkenes should be electron-rich and should be able to adopt highly ordered conformations

SCHEME 5



to cyclize to the enones efficiently. The formation of enones from δ -hydroxynitriles derived from 1-indanone and 1-tetralone offers a promising alternative for accessing 6–5–6 and 6–6–6 fused skeletons.³⁹ The cyclizations of compounds **1** and **13** are equivalent to the Robinson annulation of β -ketoesters **5** and **6** with methyl vinyl ketone (Scheme 5). The possibility of introducing different groups in the benzylic position of the bicyclic δ -hydroxynitrile makes our strategy appealing because this allows access to enones with different substituents in the α position. Moreover, this alternative takes place under conditions that could be tolerated by a variety of functional groups.

Conclusion

Our results indicate that the triflic anhydride-promoted intramolecular cyclization of δ -hydroxynitriles has potential as a new procedure for the synthesis of tricyclic ring-fused enones under simple and mild conditions. However, the structural features of the starting δ -hydroxynitriles need to be carefully

(38) To analyze the position of this equilibrium, we have studied the relative stabilities of the neutral five-membered ring imidate and its corresponding lactam, which confirmed that the latter is ca. 16 kcal mol⁻¹ more stable in the gas phase. This is in agreement with the literature. For example, see: (a) Beak, P.; Lee, J.; Zeigler, J. M. *J. Org. Chem.* **1980**, *45*, 1536–1538. (b) Overman, L. E. *Acc. Chem. Res.* **1980**, *13*, 218–224.

(39) Lomberget, T.; Bentz, E.; Bouyssi, D.; Balme, G. *Org. Lett.* **2003**, *5*, 2055–2057.

considered to avoid competition with other cyclization pathways. The pathway leading to the enone appears to be highly favored when the elimination reaction occurs readily and yields an alkene that can efficiently cyclize to the enone. The cyclizations of the 1-indanone and 1-tetralone derivatives afforded annulated enones in good yields. On the other hand, the δ -hydroxynitrile derived from 1-benzosuberone led to an imidate as the major product.

A DFT theoretical study has been performed to account for the observed reactivity pattern. The flat topology of the studied B3LYP/6-31G* potential energy surfaces suggests that slight modifications in the structures of the δ -hydroxynitriles favor one reaction channel over the other ones. The preference for the formation of the triflate over protonation is predicted to decrease along the series of compounds derived from 1-indanone, 1-tetralone, and 1-benzosuberone due to steric effects. In addition, both the ionization of the triflate to the carbocation and the subsequent cyclization of the resulting alkene become less favorable with increasing ring size. This might be explained mainly by conformational effects that produce a loss of conjugation in the carbocation and the alkene intermediates. On the other hand, the competing pathway leading to the imidate is calculated to be favored for the seven-membered ring analogue. The isomerization of the cyclic imidates under acid-catalyzed conditions might explain the formation of the lactams through an intramolecular attack of an ambident nucleophile. This pathway should be favored over the classical mechanism of the Ritter reaction, which presents a high degree of strain for this class of intramolecular processes.

Experimental Section

Representative Example for the Synthesis and the Triflic Anhydride-Promoted Cyclization of δ -Hydroxynitriles. 5-Methyl-6-oxo-6,7,8,8a-tetrahydro-fluorene-8a-carboxylic Acid Methyl Ester (15**).** To a solution of **5**^{4a} (1.6 g, 8.42 mmol) in EtOH (13 mL) were added Et₃N (2.2 mL, 15.16 mmol) and acrylonitrile (1.05 mL, 16.25 mmol). The reaction was stirred for 3.5 h and then poured into brine and extracted with Et₂O. The combined organic extracts were washed with brine, dried (Na₂SO₄), and concentrated. The residue (2 g) was submitted to chromatography, yielding **8** as an oil (1.92 g, 93%). Spectroscopic data of compound **8** were coincident to those described in the literature.^{4a} To a stirred suspension of freshly ground Mg turnings (75 mg, 3 mmol) and I₂ (one crystal) in dry Et₂O (4 mL) was added a solution of ethyl bromide (0.40 mL, 5.1 mmol) in dry Et₂O (2 mL) dropwise at room temperature. After being stirred for 30 min, the mixture was cooled

to -40°C , and a solution of ketone **8** (211 mg, 0.87 mmol) in dry Et₂O (2 mL) was added dropwise (via cannula). The mixture was then warmed to room temperature, and after 6 h a saturated aqueous solution of NH₄Cl (10 mL) was added. The layers were separated, and the aqueous phase was extracted with Et₂O. The combined organic extracts were washed with brine, dried (Na₂SO₄), and concentrated. The residue (209 mg) was chromatographed to yield **11** (128 mg, 57%) as a crystalline solid. **11**: mp 123.2–123.7 $^{\circ}\text{C}$. ¹H NMR (200 MHz) δ : 7.50–7.35 (m, 4H), 3.83 (s, 3H), 3.50 (d, J = 16.5 Hz, 1H), 2.81 (d, J = 16.6 Hz, 1H), 2.55–1.95 (m, 4H), 1.90–1.45 (m, 3H), 0.86 (t, J = 7.3 Hz, 3H). ¹³C NMR (50 MHz) δ : 174.0 (CO), 143.0 (C), 137.2 (C), 128.2 (CH), 126.5 (CH), 124.8 (CH), 124.5 (CH), 119.0 (CN), 85.9 (C), 62.9 (C), 52.0 (CH₃), 35.3 (CH₂), 30.7 (CH₂), 28.6 (CH₂), 13.3 (CH₂), 7.5 (CH₃). To a solution of Tf₂O (0.09 mL, 0.51 mmol) in CH₂Cl₂ (3 mL) at room temperature was added a solution of **11** (139 mg, 0.51 mmol) in CH₂Cl₂ (2.5 mL) dropwise. After 24 h, a saturated aqueous solution of NaHCO₃ (6 mL) was added, and the stirring was continued for further 30 min. The mixture was then extracted with Et₂O. The combined organic extracts were washed with brine, dried (Na₂SO₄), and concentrated. The residue (98 mg) was stirred in CH₂Cl₂ with silica gel overnight and then chromatographed to yield enone **15** (80 mg, 61%) as a crystalline solid. **15**: mp 107.8–109.0 $^{\circ}\text{C}$. IR (film) ν_{max} : 1660 cm⁻¹. ¹H NMR (300 MHz) δ : 7.85–7.70 (m, 1H), 7.55–7.25 (m, 3H), 3.60 (s, 3H), 3.53 (d, J = 16.3 Hz, 1H), 3.04 (d, J = 16.3 Hz, 1H), 2.75–2.65 (m, 1H), 2.63–2.50 (m, 2H), 2.30–2.10 (m, 1H), 2.17 (s, 3H). ¹³C NMR (75.5 MHz) δ : 198.6 (CO), 174.6 (CO), 156.5 (C), 145.6 (C), 139.3 (C), 130.2 (CH), 128.7 (C), 127.2 (CH), 126.7 (CH), 125.0 (CH), 55.6 (C), 52.6 (CH₃), 43.2 (CH₂), 34.7 (CH₂), 32.7 (CH₂), 11.3 (CH₃). HRMS calcd for C₁₆H₁₆O₃ (M⁺), 256.1099; found, 256.1099.

Acknowledgment. We thank Dr. Manuel González Sierra for NMR assistance, Dr. Juan Zinczuk for helpful discussion, and CONICET, Universidad Nacional de Rosario, Fundación J. Prats, and ANPCyT for financial support. V.J. thanks CONICET for a fellowship.

Supporting Information Available: Experimental procedures for compounds **16**–**21**, characterization data and ¹H and ¹³C NMR spectra for all new compounds; B3LYP/6-31G* activation and reaction zero-point corrected energies, enthalpies, and free energies in the gas phase and in solution for selected steps, Cartesian coordinates, absolute energies including ZPE, free energies in solution, and number of imaginary frequencies for all of the stationary points included in the theoretical study; values of imaginary frequencies for all of the transition structures. This material is available free of charge via the Internet at <http://pubs.acs.org>.

JO062669F